Ab initio potential energy surface of CH_2^+ and reaction dynamics of $H + CH^+$

Robert Warmbier[a] **and Ralf Schneider**[b]

This work presents a new ground state potential energy surface (PES) for CH_2^+. The potential is tested using quasi classical trajectory (QCT) and quantum reactive scattering methods for the $H + CH^+$ reaction. Cross sections and rate coefficients for all reaction channels up to 300 K are calculated. The abstraction rate coefficients follow the expected slightly decreasing behaviour above 90 K, but have a positive gradient with lower temperatures. The inelastic collision and exchange reaction rate constants are increasing monotonically with temperature. The rate coefficients of the exchange reaction differ significantly between QCT and quantum reactive scattering, due to intrinsic short-comings of the QCT final state distributions.

1 Introduction

The methylidyne cation, CH^+, is a common molecular ion in interstellar environments and comets[1]. Although it was the first cation ever identified in interstellar space[2], its dynamics of formation and destruction is not yet completely understood. In contrast to the neutral CH, its abundances can not easily be explained. One destruction channel is the collision with a neutral hydrogen atom

$$H + CH^+ \longrightarrow C^+ + H_2, \tag{1}$$

which is a reaction intuitively expected to be important, because of the high abundances of neutral hydrogen atoms in the interstellar space. This reaction is exothermic and has no known activation barrier.

Stoecklin and Halvick [3] published a potential energy surface for this reaction which was based on single electronic state *ab initio* calculations and a sixth-order polynomial fit for the three-body potential, including an *ad-hoc* term for the conical intersections. This potential was used by Halvick *et al.* [4] for quasi classical trajectory (QCT) and phase space theory (PST) analysis of the $H + CH^+$ reaction. The C^+ abstraction cross sections are predicted to be monotonically decreasing between 1 K and 1000 K. New measurements of Plasil and Gerlich[5–7] show a maximum of the rate coefficient at 60 K and a strong gradient of the thermal rate for lower temperatures, which diverges from theoretical results[3,4].

This discrepancy of experiment and theory and the unexplained abundance of CH^+ in interstellar environments motivate further research. In this work the MRCI/aug-cc-pVTZ (see 2.1) method was invoked to calculate the electronic energy for a large number of configurations. The potential energy surface (PES) was fitted using internuclear distances polynomials, adapted to account for the two conical intersections. In order to validate this PES quasi classical trajectories (QCT) and quantum scattering calculations have been performed. They give insight to the physical behaviour of the reaction and allow to derive cross sections and low temperature rate coefficients.

[a] *Max-Planck-Institut für Plasmaphysik, EURATOM Association, Wendelsteinstr. 1, 17491 Greifswald, Germany. Fax: +49 3834 864701; Tel: +49 3834 864736; E-mail: robert.warmbier@ipp.mpg.de*

[b] *Institut für Physik, Ernst-Moritz-Arndt Universität Greifswald, Felix-Hausdorff-Str. 6, 17489 Greifswald, Germany .*

2 Method

2.1 *Ab initio* calculations

Depending on the electronic structure, appropriate methods for *ab initio* calculations have to be chosen. The ground state of the CH_2^+ collisional system is A' in C_s-symmetry. Linear configurations, H-H-C and H-C-H, have the higher C_{2v} symmetry. The ground state of CH^+ is $X^1\Sigma^+$. It results in repulsive CH^+ - H potentials for linear configurations, while the CH^+ $a^3\Pi$ is attractive. This causes conical intersections to appear, which transform to avoided crossings for near-linear bend configurations. For larger bending angles the potential is purely attractive.

As the system shows a strong mixing of states, a multi-reference method, here multi-reference configuration interaction (MRCI)[8–10], has to be employed. As MRCI results depend on the symmetry used for the computation, C_s symmetry was used for all configurations. In order to represent correctly the region in the configuration space governed by the conical intersections and avoided crossings both intersecting/ avoided crossing electronic states have to be calculated simultaneously in these regions. These would be 2 A' states and 1 A'' state in C_s symmetry. Using C_s symmetry only the 2 A' states have to be calculated. Including the A'' in the optimisation process does not improve the A' state energies. Far outside the crossing regions only the lowest electronic state is of interest, yet both A' state have been computed over the whole configura-

tion space to avoid discontinuities in the regions where energies are computed in two different ways, meaning with one or two states of the same irreducible representation included in the optimisation process. This can happen as the starting orbitals from the MCSCF calculation (see below) are different for these cases.

The choice of active space and basis sets is a compromise between accuracy and speed. In this case, we aimed at a convergence threshold respective to basis sets and active space of less than the typical error of our fitting procedure. This can be estimated to be several 10^{-4} hartree, which corresponds to about 10 meV. We chose the augmented correlation-consistent valence triple zeta (aug-cc-pVTZ) basis sets of Dunning [11,12]. A larger basis like aug-cc-pVQZ would have been too expensive. The non-augmented cc-pVQZ basis has a size between aug-cc-pVTZ and aug-cc-pVQZ. The augmented versions of Dunning's basis sets have additional diffusive terms [12]. These terms can be important in the pre-dissociation phase and for non-localised or weakly bound electrons. The cc-pVQZ basis was ruled out, because it lacks these diffusive terms.

For each configuration, first complete active space self-consistent field [13,14] (CASSCF) orbitals and electron densities are calculated. As the lowest two A' states are included in the calculation, these orbitals and densities are state averaged (SA-MCSCF) with equal weights for each state. The innermost *s*-shell of C is considered closed, leaving 5 electrons to be distributed over 10 active molecular orbitals (8 A', 2 A''). In the following, Davidson-corrected internally-contracted multi-reference configuration interaction [8–10] (MRCI) was used, where both states were optimized simultaneously with the C 1s electrons treated as core. All *ab initio* calculations were performed using MOLPRO2009.1 [15].

2.2 Potential energy surface

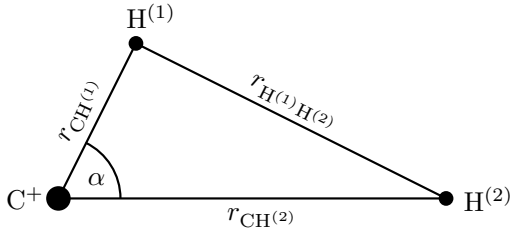

Fig. 1 Sketch of coordinates used to describe the CH_2^+ molecular system.

The potential energy surface (PES) is constructed following Braams *et al.* [16–20] and Murrell *et al.* [21]. In the original ansatz, the potential energy surface is fitted in terms of polynomials of exponential functions of internuclear distances, $y_{ij} = \exp(-r_{ij}/\lambda)$, where λ is a scale parameter and i and j are nuclear indices. The polynomials are restricted to be invariant under permutation of identical nuclei, which is built into the basis. The coefficients in the polynomial expansion are determined by solving a weighted least squares system of equations in which we assign to the k-th configuration a relative weight $(E_k - E_0)/(E_k - E_0 + \delta)$. E_k is the *ab initio* energy of the configuration, E_0 is the *ab initio* energy at the global minimum, and δ is a parameter for which we used 0.05 hartree.

The standard form of the PES is well-suited for single-valued global potentials without cusps. In order to account for conical intersections this approach has to be modified. Our need is a representation for the conical intersection, which smoothly transforms into an avoided crossing form at near-linear configurations. It is reasonable to stay with the well-tested potential and to add another set of polynomials for each intersection. These should be non-zero only in the vicinity of the corresponding intersection. Using this approach one has the full flexibility to choose appropriate functions/functionals for the intersections, while keeping all advantages of the well-known PES, including the simultaneous least-squares fit of all coefficients. In the case of a x_2y_1-type system the internuclear distances are $r_{x^{(1)}x^{(2)}}$, $r_{x^{(1)}y}$, $r_{x^{(2)}y}$, as shown in figure 1 for CH_2^+, and the invariant basis is $r_{x^{(1)}x^{(2)}}$, $\overline{r_{x^{(i)}y}}$ and $\overline{r^2_{x^{(i)}y}}$.

This work uses the standard variable transformation $y = e^{-r/\lambda}$ for the *xy*-distances, the *xx*-distance is transformed as

$$y = e^{-|r-r_0|/b}, \tag{2}$$

where r_0 is the position of the conical intersection, which might depend on the other coordinates as well. It is best to use first or second degree polynomials with these coordinates, otherwise a poorly chosen r_0 might produce erratic behaviour of the fit close to r_0. In addition to the modified polynomial a modified damping function was introduced:

$$t_0 = e^{-k*\min(\alpha,\pi-\alpha)} \max\left(e^{-l|r_{x^{(1)}y}-a|}, e^{-l|r_{x^{(2)}y}-a|}\right). \tag{3}$$

α is the angle x-y-x , which can be easily calculated from the internuclear distances. The chosen form of the potential near the intersection is very sensitive to the parametrisation, but it offers a representation of intersections with an accuracy similar to the accuracy of the potential fit.

The overall computational cost of the added polynomials is insignificant compared to the original PES, which can use polynomials up to 19th order for triatomic systems.

2.3 Dynamics

The quasi classical trajectory method (QCT) was applied for the calculation of cross sections and rate coefficients. A code

was developed using fifth-order Gear[22] predictor-corrector integration and adaptive time-step management. The initial conditions calculation were implemented using the semi classical Einstein-Brillouin-Keller quantisation of the action integral. As the particles are moved by Newton's equations of motion in QCT, no quantisation of vibration or rotation is preserved over the trajectories. Especially in the case of low kinetic and internal energy, where the vibrational zero-point energy is a large fraction of the total energy, quantum-mechanically forbidden results dominate.

In the standard weighting each quasi classical trajectory has a weight of unity and product quantum numbers for final state resolved cross sections are given by the nearest integer to the semi classical ones. Bonnet[23–26] suggested a modified treatment for inelastic collision calculations, where the product state rotational distributions have to be corrected in the standard QCT. Starting from the classical S matrix theory (CSMT), see e.g. the work of Miller and Marcus[27–29], the product side state distribution is expressed in terms of Dirac distributions. Cross sections deduced at this point are exact in the context of CSMT, if the contribution from the interference term of the semi classical probability is negligible (see Bonnet[23] equations 4 and 6). The set of trajectories with integer semi classical quantum number is usually of zero measure with respect to the set of all trajectories. In order to compensate that the Dirac distribution is substituted by a Gaussian distribution, whose width have to be small to mimic the Dirac distribution. With this Gaussian weighting (GW) or binning used for the product state vibrational quantum number the cross sections for channels α are calculated as

$$\sigma_\alpha^{GW} = \pi b_\alpha^2 \frac{N_c}{N} \frac{w_\alpha}{w_c}, \tag{4}$$

where N is the total number of trajectories with impact parameter $b \leq b_\alpha$, the largest impact parameter leading to channel α. The complex-forming trajectories N_c include non-elastic collisions and chemical reactions, which form the channels α, as well as an elastic component. The weights $w_\alpha = \sum_i^{N_\alpha} w_i$ and $w_c = \sum_i^{N_c} w_i$ are calculated using the Gaussian weighting approach. The Gaussian is defined as

$$w_i(\delta v_i;\alpha) = \frac{1}{\sqrt{2\pi} s_\alpha} e^{-\frac{(\delta v_i)^2}{2 s_\alpha^2}}, \tag{5}$$

where δv_i is the difference between the final vibrational quantum number and its nearest integer value of trajectory i and s_α^2 is the variance of the Gauss function for channel α.

The Gaussian weighting does not necessarily provide satisfactory results when the width of the Gaussian can not be chosen small enough or when the CSMT is failing. For this system we found GW-QCT to give a too strong weight on exchange cross sections and a too low abstraction cross sections, especially for the cases with larger energies, where the weighting should have less influence. This effect can also be seen for the rate coefficients in figures 9 and 10. Therefore, we introduced an empirical modification (mQW) to the original Gaussian weighting, with the aim to prevent forbidden low energy paths to be populated but to use larger s_α for larger energies to improve the agreement with the quantum mechanical results. We will use s_α to adapt the width of the weighting function for each channel separately.

Let us approximate the rotational energy of the diatomic product as a rigid rotor with $E_{rot}(j) = Bj(j+1)$ and the vibrational energy as a harmonic oscillator $E_{vib} = \omega(v+\frac{1}{2})$, with rotational constant B, harmonic frequency ω, rotational and vibrational quantum numbers j and v. The difference of the vibrational energy from the integer quantum number value δv should be less than the smallest rotational transition energy: $\omega\,\delta v < 2B$. As in our case the Gaussian weighting is meant to prevent the population of closed channels, an effective weighting follows $s_\alpha \propto B_\alpha/\omega_\alpha$. An appropriate proportionality factor has to be chosen manually, yet it can not be much larger than unity as the weighting would allow forbidden low energies transitions. An additional discussion about the different QCT weighting schemes can be found in appendix A.

It is also possible to use Gaussian weighting for the final rotational quantum number as well. Tests have shown no significant change in the cross sections for rotational weighting widths s_J in the order of 10^{-1} and a strong gradient in the cross sections depending on s_J, if it's chosen in the order of 10^{-2}, with no sign of convergent behaviour. Therefore, this work is not using rotational weighting.

To obtain an error estimate of equation (4) error propagation of independent variables is used. $f(x_i)$ being a function of independent variables x_i and their standard deviations Δx_i, the deviation Δf is given by

$$\Delta f = \sqrt{\sum_i \left(\frac{\partial f}{\partial x_i}\Delta x_i\right)^2}. \tag{6}$$

The maximum impact parameter b_α is obtained from the trajectory calculations. Assuming that all reaction channels α need a complex formation, the maximal impact parameters of all these channels should be identical. Therefore, the standard deviation of the impact parameter can be calculated directly. The first addend for the error propagation is therefore $\left(\frac{2\Delta b_\alpha}{b_\alpha}\right)^2 \sigma_\alpha^2$. N and N_c are dependent variables as $N = N_c + N_n$, where N_n is the number of non-complex-forming trajectories with $b \leq b_\alpha$. As these variables represent the convergence of a Monte-Carlo process, their error can be estimated by their square root, e.g. $\Delta N_c = \sqrt{N_c}$. This yields $\frac{N-N_c}{N_c N}\sigma_\alpha^2$ as the second term in the error propagation. This term converges with $1/N$. We have chosen to use two terms for the error estimate of w_α and w_c. As the weights are calculated over finite sums with upper bounds N_α and N_c, respectively, we apply the same

scheme as for the error estimates of the N's. The third term of the error propagation is therefore $\frac{w_c - w_\alpha}{w_\alpha w_c}\sigma_\alpha^2$. Using both terms, for N and w, yields a small overestimation of the error, as N_c and w_c are not independent. This overestimation is negligible for small $\sqrt{1/N_c}$. Another uncertainty lies in the definition of the w_i in equation (5). The parameter s_α has no analytically defined value. The sensitivity of the cross sections to the choice of s_α is included by a separate term in the error propagation calculation. We defined normalised weights $\Omega_\alpha = \frac{w_\alpha}{w_c}$. We then used the standard deviation of Ω_α with respect to changes of s_α. This does not necessarily measure the convergence, but rather the slope of the s_α dependency of the cross sections. All these terms result in a variance estimate for σ_α given by

$$s_{\sigma_\alpha} = \sigma_\alpha \sqrt{\left(\frac{2\Delta b_\alpha}{b_\alpha}\right)^2 + \frac{N - N_c}{N_c N} + \frac{w_c - w_\alpha}{w_\alpha w_c} + \left(\frac{\Delta\Omega_\alpha}{\Omega_\alpha}\right)^2}. \tag{7}$$

Assuming an equilibrated Boltzmann distributed system at temperature T, the thermal rate coefficients $\kappa_\alpha(T)$ are

$$\kappa_\alpha(T) = \left(\frac{8}{\pi\mu(kT)^3}\right)^{1/2} \int_0^\infty E_{coll} e^{-E_{coll}/kT} \sigma_\alpha(E_{coll}, T) \mathrm{d}E_{coll}, \tag{8}$$

with temperature averaged cross sections

$$\sigma_\alpha(E_{coll}, T) = \frac{1}{Q_\alpha} \sum_n g_n \sigma_\alpha(E_{coll}, n) e^{-E_n/kT}, \tag{9}$$

where $n = \{v, j\}$ represents the internal degrees of freedom and $\sigma_\alpha(E_{coll}, n)$ are the initial-state resolved cross sections depending on the collisional energy E_{coll}. Further quantities are the reduced mass μ, the multiplicity g_n of state n and the canonical partition function Q_α. For cross checking the low temperature results obtained with QCT with full quantum mechanical results, a modified version of the ABC[30] quantum scattering code was used. This program solves the Schrödinger equation of the atom-diatom chemical reaction with a coupled-channel hyper spherical coordinate method. While the quantum scattering approach is more confidable than the QCT method, computational costs grow too large for higher energies, as more states get involved. This restricts the application to low temperature bench marking.

3 Results

3.1 Potential energy surface

The CH_2^+ potential energy surface for the lowest A' electronic state was built from 16259 *ab initio* points. The standard polynomial was built with 5th order two-body polynomials and 13th order three-body polynomials. The cut-off lengths were chosen to be 12 and 8 a_0, respectively. The additional polynomials were both chosen to be 2nd order. The 0 eV-level is set to the asymptotic $H + CH^+$ energy for the whole work. A complete list of parameters and coefficients are given by request.

The weighted root mean square (rms) error of the PES is 6.3 meV. The rms error for energies smaller than 0.1 hartree (0.1 hartree $\approx$ 2.7 eV) above the global minimum is 15.5 meV and for energies between 0.1 and 0.2 hartree above the global minimum it is 17.2 meV. This means, that in the incoming channel variations due to errors in the fitting with amplitudes in the order of 10 to 20 meV have to be expected. These variations have their origin in the polynomial form of the fitting function. If the kinetic energy is larger than this, the fragments are decelerated, accelerated and possibly deflected, but not reflected. Therefore, the reactive behaviour should not change significantly. If an incoming hydrogen hits a positive hump with a kinetic energy lower than the height of the hump, it is going to be reflected, causing a corruption of the reaction statistics. A symptom for this would be an otherwise unexplained increase of elastic scattering events for collision energies of less than 20 meV. Other important quantities of the PES are given in table 1. The equilibria of the complex and the different fragments differ between $0.005\,a_0$ and $0.02\,a_0$ with the experimental data, the dissociation energies up to 0.06 eV. The exoergicity of 0.518 eV is near the experimental value of 0.496 eV. This is well within the expected limits of the MRCI/aug-cc-pVTZ method and comparable with Stoecklin and Halvick , where bond lengths are underestimated and dissociation energies are overestimated. This work shows opposite behaviour with underestimated dissociation energies and partly overestimated bond lengths. For the complex region this work better fits experiments, but the fragments are slightly better represented by the former work, which is probably caused by the form of the fitting functions.

The validity of the extended fit using additional polynomials to describe the conical intersections can be shown visually. Figure 2 shows one-dimensional cuts through the PES for an incoming H atom with CH^+ at equilibrium distance in the collinear C-H-H and H-C-H cases. From the *ab initio* data it can be seen how the two lowest A' electronic states cross at the upper end of the potential well causing a small hump if

Table 1 Important reference values of the PES with experimental values in brackets: Dissociation energies D_e, equilibrium bond distances r_e and angles α_e. CH_2^+ dissociation energy to $CH^+ + H$.

	D_e / eV	r_e / a_0	α_e
CH^+	4.195 (4.255)	2.142 (2.137)	—
H_2	4.711 (4.751)	1.412 (1.401)	—
CH_2^+	4.778	2.069 (2.088)	141.2° (139.8°)

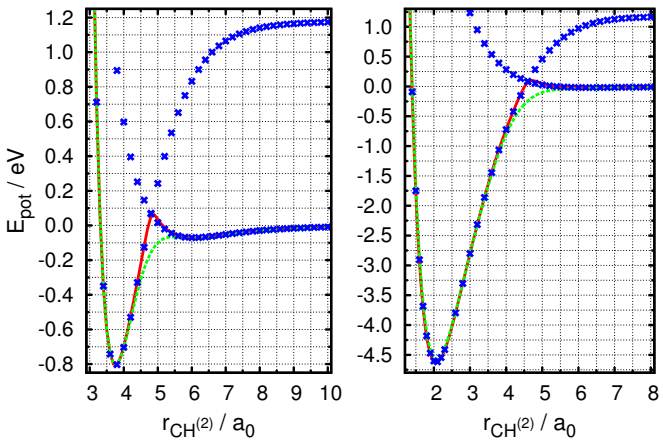

Fig. 2 One-dimensional PES cut for fixed $r_{\mathrm{CH}^{(1)}} = 2.14\ a_0$ at linear C-H-H (left) and H-C-H (right) configuration. Crosses: *Ab initio* energies for the lowest two A' states. Line: PES with additional terms. Dashed line: standard PES.

one follows the lowest energy path over $r_{\mathrm{CH}^{(2)}}$. The standard polynomial form of the PES can not reproduce this form and gives a fit "ignoring" this feature. The additional polynomials are able to compensate this shortcoming. The fit in figure 2 satisfactorily matches the intersections with corresponding heights of 68 meV and 99 meV above the asymptotic energy value, although the intersections are not spiky but smoothed.

Another overview over the incoming channel is given in figure 3, where $r_{\mathrm{CH}^{(1)}} = 2.14\,a_0$ is fixed again and the potential is given as a function of $r_{\mathrm{CH}^{(2)}}$ and α. Figure 3(a) shows an overview over the complete channel, while figure 3(b) shows a more detailed map of the far-field potential of the incoming channel. If the H atom is approaching towards the bounded H atom, attractive forces are weaker compared to the approach towards the C atom. CH^+ has one free $2p$ orbit compared to its neutral counterpart. This yields a high overall electron affinity of the system, but the attractivity is mostly located at the C atom. The conical intersections for both collinear configurations can clearly be seen. Due to the avoided crossings at near linear configurations and the attractive character of the potential for bent configurations a clear gradient towards bent complex configurations around 80° to 160° appear. There is no barrier for an incoming projectile preventing the formation of a CH_2^+ complex, except while entering and staying in a collinear configuration, which is an unlikely event. The far-field interaction between CH^+ and H is crucial for the low temperature reactive behaviour. Therefore it has to be proven, that no artificial undulations are erected by the fitting procedure. For an incoming H atom the potential is purely attractive for all except near linear configurations. Around the 0° limit the potential is attractive for $r \geq 6\,a_0$, as can be seen in figure 2. The hump caused by the conical intersection reaches a height larger than the asymptotic energy limit for up to 7° of bending. At the 180° limit, the hump of the conical intersection is $> 0\,\mathrm{eV}$ up to a bending angle of 168° . For this limit a region approximately between $9\,a_0$ and $11\,a_0$ has a potential value higher than the asymptotic limit with a maximum of 1.5 meV. This is an artefact of the fit. Due to the small amplitude and the narrow angular spread of this feature, the influence on the chemical dynamics should be negligible. Other artificial

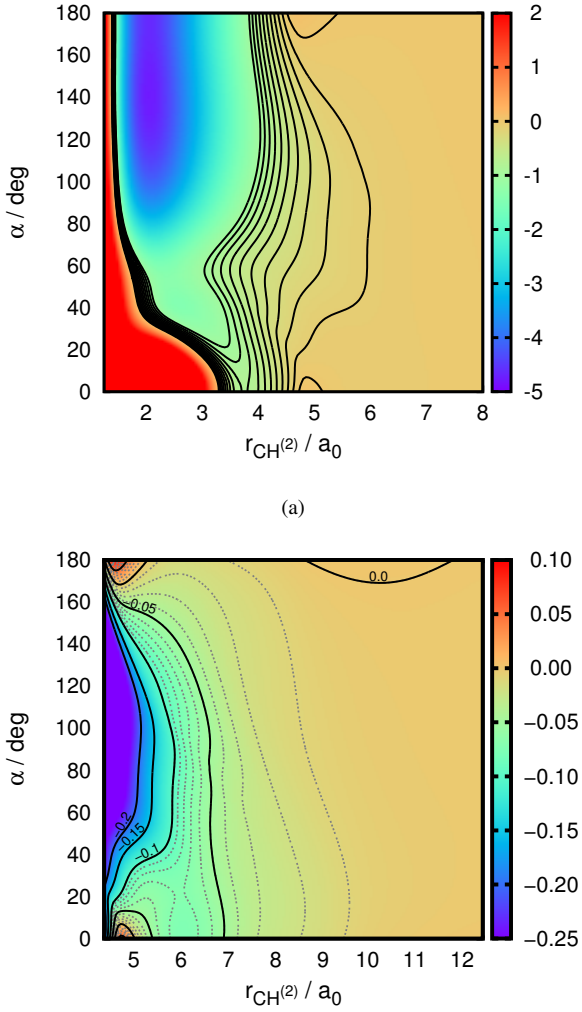

Fig. 3 Two dimensional PES cut for fixed $r_{\mathrm{CH}^{(1)}} = 2.14\ a_0$.
3(a): Contour lines between -1.0 eV and 0.1 eV are drawn with an increment of 0.1 eV.
3(b): Contour lines (black) are drawn between -0.2 eV and higher with an increment of 0.05 eV and (gray dashed) between -0.1 eV and 0.1 eV with an increment of 0.01 eV.

undulations were not found using contour plots of the incoming channel with a resolution of up to 5 meV. This implies, that classical trajectories with a projectile kinetic energy of at least 5 meV should not be compromised by the PES. A more detailed discussion of the influence of the PES on the dynamics can be found in Appendix B.

3.2 Cross sections

3.2.1 Quasi classical trajectory. Initial state selected cross sections from 4.0 million QCT trajectories have been computed for $J = 0, \ldots, 10$ and collision energies of 1, 2, 4, 8, 16, 30, 60, 100 and 200 meV. For the standard Gaussian weighting (GW) we used $s_\alpha = 0.002$ and for the modified version mGW $s_\alpha \sim B_\alpha / k_\alpha$, resulting in $s_\alpha = 0.004$ and 0.015 for CH^+ and H_2 forming channels, respectively, for the lowest energy initial conditions. For initial conditions with higher energy such small weighting widths are not necessary as the rotational level splitting increases and therefore more energy has to be transferred from the zero point energy to the rotational degree of freedom to open a closed rotational energy path. In addition, a small weighting width diminishes the statistics. Therefore, the width was increased for initial conditions with higher energy, such that the quantum mechanical results are resembled as good as possible. As the s_α for the abstraction channel in mGW-QCT is chosen significantly larger than for the other channels mGW-QCT will automatically have stronger abstraction cross section than GW-QCT. Figures 4, 5 and 6 show selected mGW-QCT cross sections for inelastic collisions, H exchange and C^+ abstraction, respectively, for the different initial rotational states as a function of the collisional energy. The error bars are the $2s_{\sigma_\alpha}$ confidence intervals obtained from equation (7). This error estimate is dominated by the weight w related term. The b_α and N related terms are smaller than $0.025\,\sigma_\alpha$ and $0.004\,\sigma_\alpha$, respectively. The Ω_α related term, which accounts for the s_α parametrisation is large, up to $0.33\,\sigma_\alpha$, for small total energies. There the energy differences between rotational states are small and a smaller s_α would be needed. Yet, this would lead to a worse convergence of w, which would require more trajectories to be calculated than feasible.

The behaviour of the cross sections in dependence of the rotational state of the reactants and the collisional energy is a superposition of the dependence of the maximal impact parameter and the relative probabilities. The maximal impact parameter is decaying for increasing collisional energy from roughly $12.6\,a_0$ (J=1) to $7.2\,a_0$ (J=10) for 200 meV. This is expected, as higher relative velocities decrease the interaction between the far field potential of the target and the projectile, reducing the deflection of the projectile. We also see a small variation of the maximum impact parameter for different J, yet this effect is small with changes of about $0.2\,a_0$. The maximum impact parameter for all collisional channels are identical for almost all cases. Their deviation is usually less then 1%, which is well within the convergence limit uncertainty. This implies that all these channels appear after experiencing complex formation. The impact parameters for $J = 0$ differ for collisional energies ≤ 8 meV from the smooth behaviour of the rest of the parameter space. The impact parameters of 4 meV and 8 meV are $0.7\,a_0$ and $0.3\,a_0$, respectively, larger than their corresponding $J = 1$ counterparts. The 1 meV impact parameter is $0.3\,a_0$ smaller then the $J = 1$ value. Comparisons with quantum scattering results (see 3.2.2) indicate that these impact parameters are no artefacts of the QCT method, but a characteristic of the PES. Lowered impact parameters for small kinetic energies can be produced due to variations in the PES, as mentioned before.

Another important factor is the partition function. The first rotational level of CH^+ has a rotational energy of about 3.5 meV. If the total energy is less than this, no inelastic collision can happen and the H-exchange reaction has only one energetic path. If the energy increases more paths open, yet the inelastic case has always less paths available than the exchange case. The situation for the C^+-abstraction is rather different, as the product composition is different. H_2 has a smaller zero-point energy compared to CH^+, allowing several paths even for low collisional energies. On the other hand the rotational level splitting is larger, thus the increase of open paths with higher energies is slower than for the other reaction channels. If not governed by other factors, cross sections should decrease with larger collisional energy. The abstraction cross section should be large for small total energies and decrease with larger energies. Inelastic and exchange cross section should be zero or small for low energies and increase with larger total energy. Both cases should behave similarly.

Figure 4 shows initial-state selected inelastic collision cross sections. The $J = 0$ cross section increases monotonically from almost zero to approximately $80\,a_0^2$ between 60 meV and 100 meV and then decreases slightly again in agreement with our expectations. The low energy cross sections increase with increasing J and reach a quasi constant level for $J \geq 5$. There the cross sections are slowly decreasing with collisional energy. The upper bound is not explained by our arguments given before and is discussed later.

The H-exchange cross sections in figure 5 show, as expected, a similar behaviour like the inelastic collisions, but with some considerable differences. The cross sections start to decrease, partly very fast, for collisional energies larger than 30 meV. This is for lower energies and more pronounced than in the inelastic case. For $J \geq 7$ cross sections start decreasing again, while they stay at the same level for inelastic collisions.

The C^+ abstraction cross sections (Fig. 6) are generally large at low energies with a maximum of $350\,a_0^2$ and decrease to higher kinetic energies. This is expected by the kinetic and

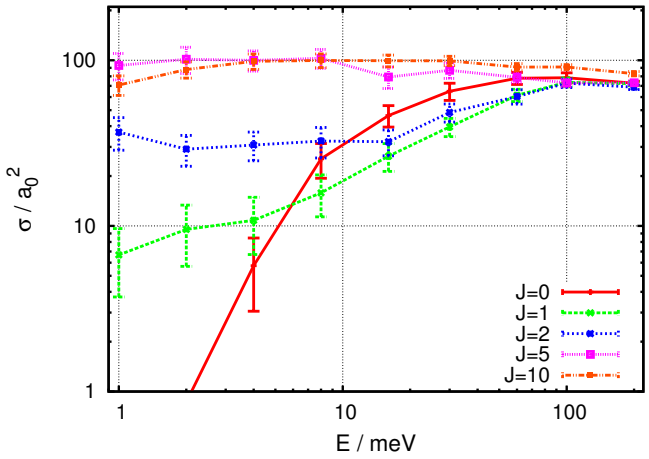

Fig. 4 QCT, with Gaussian weighting (mGW-QCT), inelastic collision cross sections for several values of the rotational quantum number J versus the collision energy.

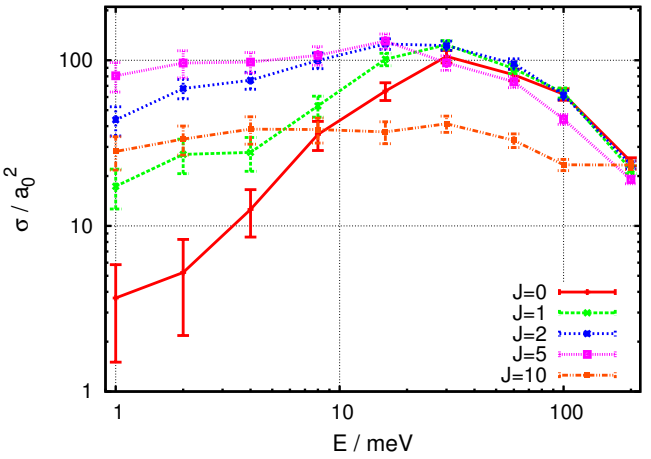

Fig. 5 QCT (mGW-QCT) H exchange reaction cross sections for several values of the rotational quantum number J versus the collision energy.

partition considerations. In addition the cross sections are decreasing for increasing J up to $J = 7$, afterwards they increase slightly again.

For rotational or translational energies larger than approximately 100 meV inelastic cross sections grow larger than exchange cross sections. For this, the life-time in the complex has to be looked at. While most of the trajectories have life-times in the order of 10^2 fs, the range goes from few 10^1 fs to $1 \cdot 10^4$ fs. While the average time in the complex decreases slightly with larger total energy a minimum time is still needed to form exchange or abstraction products. In contrast to that, higher energies yield an increasing number of trajectories with complex times shorter than this threshold, which result in inelastic collisions.

A possible explanation for the switching (increase/ decrease) behaviour with changing J is rotational shielding. The center-of-mass for CH^+ is near the carbon ion. If brought into rotation the hydrogen is shielding the carbon, changing the probabilities, whether an incoming projectile is hitting one or the other. For higher kinetic energies of the projectile this is compensated. It is plausible to assume, that after a certain point, the shielding reaches an optimum and can not be improved further. Previous publications[4,31,32] claim, that the rotational shielding prefers the product channels with light atom separation.

3.2.2 Quantum scattering. As the reliability of QCT cross sections strongly depends on the weighting, the number of trajectories and whether additional quantum mechanical effects are important a cross check with another method is useful. A series of quantum scattering calculations using the ABC code were performed. The initial diatomic rotational quantum number was restricted to $J \leq 5$. Figure 7 shows a comparison of mGW-QCT and ABC low energy abstraction cross sections. For $J = 0$ to 2 the QCT results are mostly following the ABC results. Both method yield similar results here. For $J = 3$ to 5 QCT cross sections are generally larger than the ABC results. The good agreement for small rotations implies, that the weighting width was chosen appropriately. Also the slope for larger rotational energies is satisfactory. Differences of the absolute values are to be expected when comparing results from different methods.

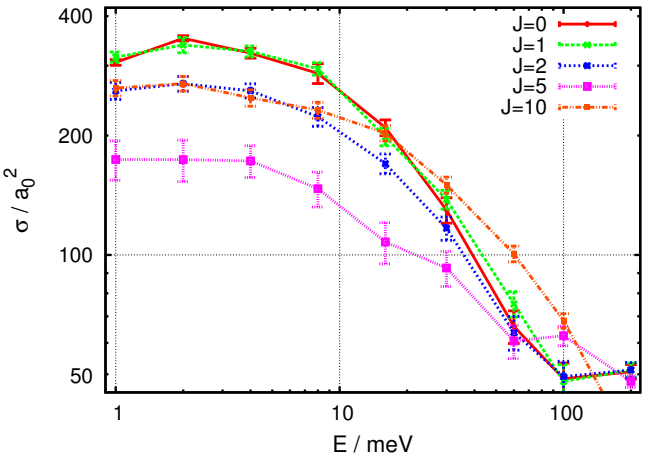

Fig. 6 QCT (mGW-QCT) C^+ abstraction reaction cross sections for several values of the rotational quantum number J versus the collision energy.

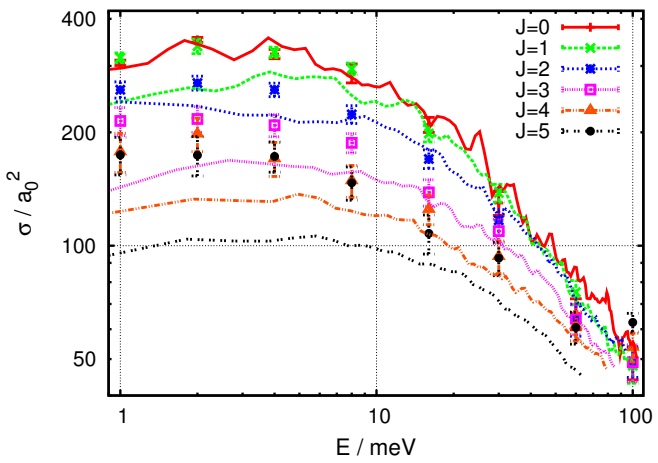

Fig. 7 Low energy C^+ abstraction cross sections from mGW-QCT (dots with error bars) and ABC (lines) calculations.

3.3 Rate coefficients

The energy range chosen in this work allows to calculate rate coefficients up to 300 K. As we calculated cross sections only for energies of 1 meV and larger, their dependence of smaller energies is unknown. Therefore, we calculated several low temperature limits (linear, constant, divergent), where the constant and divergent limits give almost identical results. With the exception of inelastic collisions, which do not appear for the low temperature limit, we give maximal corrected rates as an upper bound for the real value. QCT reaction rate coefficients are given for standard histogram binning (HB-QCT), Gaussian weighting (GW-QCT) and the modified Gaussian weighting (mGW-QCT). ABC cross sections were calculated up to 60 meV only. Therefore, we restricted the ABC rate coefficients to 150 K. We compare our results with previous published numerical work of Halvick *et al.* which is based on the Stoecklin and Halvick PES. They used GW-QCT as well as phase space theory (PST) methods. Their maximal cross sections are larger, implying a larger maximal impact parameter of at least $25\,a_0$, which is approximately twice the size as ours.

Figure 8 shows inelastic collision rates from QCT and ABC calculations compared to QCT results of Halvick *et al.*. The Halvick *et al.* coefficients are larger than the ones from this work, besides the HB-QCT results, which are intrinsically overestimates for this system. ABC, GW-QCT and mGW-QCT results are similar. The results of Halvick *et al.* are generally larger with decreasing difference for higher temperature due theit larger low energy cross sections. Therefore, it originates from an area of the parameter space, where both potentials can not be considered as reliable.

The picture for the exchange reaction is looking rather different, as can be seen from figure 9. Here, we find quite good agreement between PST, HB-QCT and ABC results, while all weighted QCT results are off. Our GW- and mGW-QCT results have a too steep slope and a high temperature limit, which is almost twice as high as PST and ABC results. The low energy mGW-QCT cross sections are too small compared to the ABC ones. On the other hand we find too large high energy cross sections. It seems that Gaussian weighting distorts this particular channel, while the other two are improved over HB-QCT.

Previous numerical results show a monotonic behaviour for QCT and PST abstraction rate constants. This is in agreement with theoretical expectations and experimental results, e.g. from Luca *et al.* [33] and Federer *et al.* [34,35]. Our QCT and ABC results are generally lower than the results of Halvick *et al.*. Both numerical works agree on the same level with experiment, although they are separated by a factor of two. Our results show a different behaviour for temperatures lower than 50 K as they have a positive slope there. Plasil *et al.* [5,6] have found a similar behaviour. They measured abstraction cross sections which have a strong gradient for temperatures less than 50 K. The rate at 12.2 K, for example, is about $5 \cdot 10^{-11}\,\mathrm{cm^3 s^{-1}}$. Although we find a drop of the reaction rate for low temperatures, this strong decrease could not be reproduced, except for HB-QCT. Yet HB-QCT underestimated the low temperature rate coefficients as it underestimates the corresponding cross sections. Our lower reaction rate coefficients for low temperatures are caused by the relative small impact parameter at low kinetic energies, which are defined by the far field potential.

All cross section and rate coefficient data (ABC,

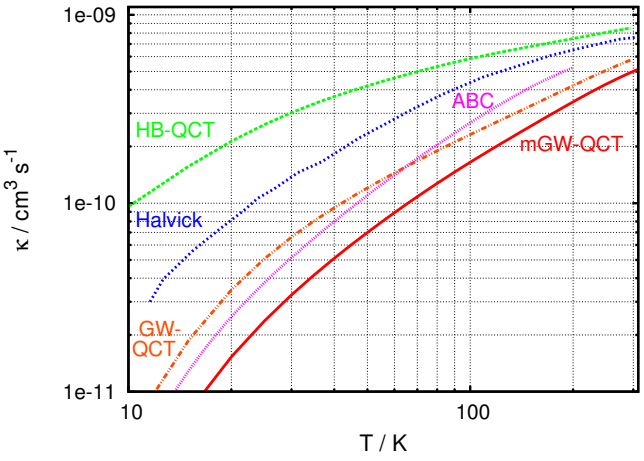

Fig. 8 QCT and ABC rate coefficients for the inelastic collision channel. For comparison the QCT results of Halvick *et al.* are given.

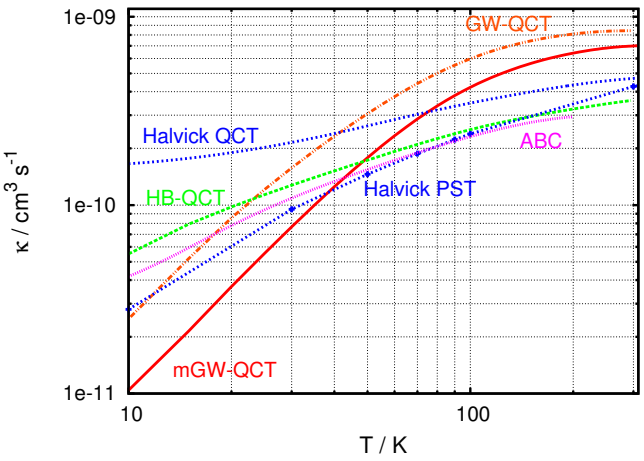

Fig. 9 QCT and ABC rate coefficients for the exchange reaction channel. QCT and PST rate coefficients from Halvick *et al.* are shown as well.

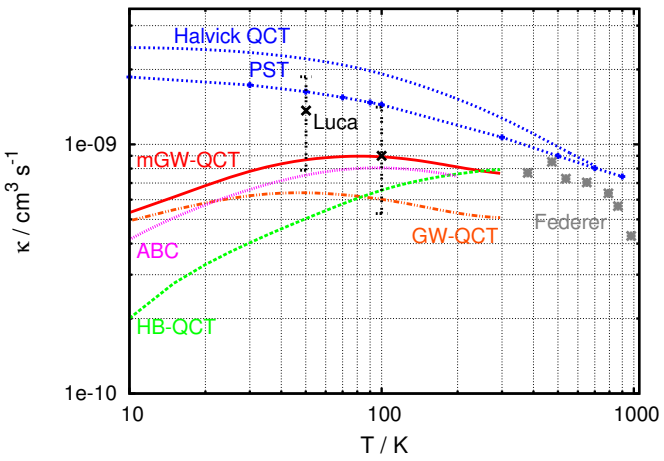

Fig. 10 QCT and ABC rate coefficients for the abstraction reaction channel. QCT and PST rate coefficients from Halvick *et al.* are shown as well. Experimental rate constants from Luca *et al.* and Federer *et al.* are also included.

HB-QCT, GW-QCT, mGW-QCT) is available online at www.rzg.mpg.de/˜rfs/ch2p/.

4 Conclusions

A new potential energy surface for the $H + CH^+$ reaction was developed. It shows good agreement with experimental data and previous numerical results within the accuracy of the methods implied.

Discrepancies between different numerical studies indicate a high sensitivity of low temperature reaction rates to the electronic potential used. Fitted *ab initio* potentials have fitting errors in the order of 10 meV. Depending on the functional form used, the far field potential can be distorted from the underlying *ab initio* data by several meV. This can deteriorate low kinetic energy dynamics using such a potential. The potential used in this work has a root mean square error of about one order of magnitude smaller than the one of Stoecklin and Halvick. We used a smaller Gaussian weighting width than Halvick *et al.* and therefore reduced the weighting errors for low energy cross sections. Therefore we consider this work a significant improvement. Yet, we acknowledge, that further research is necessary to develop a potential suited for low energy dynamics without restrictions.

Our results indicate the possibility of an inhibited abstraction reaction for low temperatures, yet more accurate electronic potentials are needed to quantify and verify this.

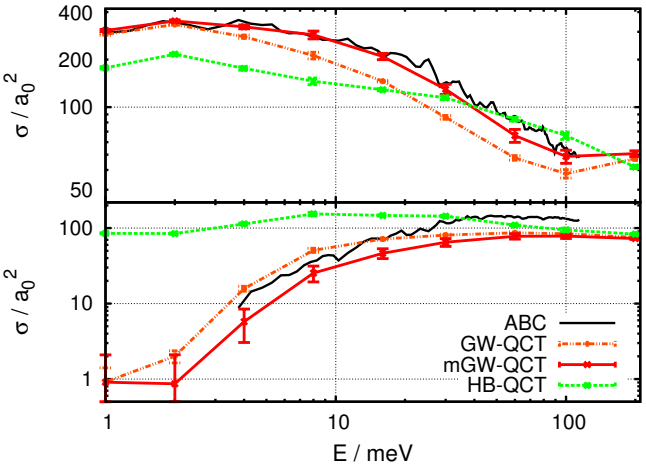

Fig. 11 Comparison of J=0 QCT cross sections (Upper plot: abstraction, lower plot: inelastic collision.) for different weighting techniques with ABC quantum scattering results as reference. For a description of the techniques see the text.

Appendix A

The analysis and interpretation of QCT results is sometimes difficult as the classical dynamics do not preserve integer quantum numbers or zero point energy. Especially in low energy cases this shortcoming can seriously deteriorate results. The original approach is to give each trajectory a weight of unity and therewith merely counting trajectories. The cross

section are then given by

$$\sigma_{\alpha}^{HB} = \pi b_{\alpha}^{2} \frac{N_{\alpha}}{N}. \quad (10)$$

Within this histogram binning (HB) final state resolved cross sections can only be calculated with tagging each trajectory with the nearest integer quantum number. As can be seen in figure 11 the histogram binning inelastic collision cross sections are relatively constant for collision energies between 1 meV and 100 meV, while the ABC quantum scattering cross sections are zero for energies below 3.45 meV, increase strongly up to 50 or 60 meV and afterwards stay constant or decrease slightly. The low energy QCT histogram binning cross sections overestimate channels near the zero point energy and even allow energetically forbidden paths due to forbidden energy transfers from the zero point vibration to the rotational degree of freedom. This also leads to an underestimation of low energy abstraction cross sections. Obviously, an alternative treatment has to be found.

One approach is to weight trajectories according to their deviation from integer quantum numbers (see section 2.3 for details). Theoretically, this Gaussian weighting[23–26,36] should eliminate "wrong" trajectories from the set and therefore improve the cross sections. Yet, this is only true for the limit of very small weighting widths, where only trajectories with almost integer quantum numbers are left. This set is small for small s_{α} and probably empty in the limit of the Dirac distribution. A tremendous amount of trajectories have to be calculated to gain a reasonable set size. A small set on the other hand introduces statistical errors. Medium weighting widths, which decrease the influence of false trajectories but keep a reasonable large set have to be used. While the Gaussian weighting is physically motivated, it does not necessarily deliver accurate results. This can be the case, if the classical S matrix theory does not adequately describe the system at hand. It is also possible that one can not calculate enough trajectories for an sufficient small weighting width. The GW-QCT curve in figure 11 is calculated with $s_{\alpha} = 0.002$ for all trajectories. This is roughly a factor of 8 smaller than the one used by Halvick *et al.*. As can be seen, the low energy inelastic cross sections are decreasing by almost a factor of 100 to approximately $1 - 2\,a_0$. The cross sections should be zero below 3.45 meV. This is a difficult case for any statistical technique, as the set of (allowed) trajectories for low energies is zero for some channels. If the conditions are not rigorous, e.g. Gaussian instead of Dirac distribution, these cross sections are naturally very noisy. The general form of the cross sections has improved considerably, yet the abstraction cross sections are underestimated by the GW-QCT. The high energy abstraction cross sections get deteriorated by the weighting as an artificial minimum appears.

To further improve this we introduced a weighting width which is similar to the ratio of rotational and vibrational constants for each channel, as described in 2.3. This purely empirical treatment was chosen to prevent the population of forbidden final states. While this method efficiently erases forbidden reaction paths from the set, there is a risk of artificially preferring channels by the unequal weighting. Using values of $s_{\alpha} = 0.004$ and 0.015 for CH^{+} and H_2 forming channels, respectively, we get the mGW-QCT curve in figure 11. The s_{α} are increased linear with the energy. In this case, the abstraction cross better fit to the ABC results. Yet, neither QW-QCT nor mGW-QCT could deliver a constant quality for all calculated cross sections.

Appendix B

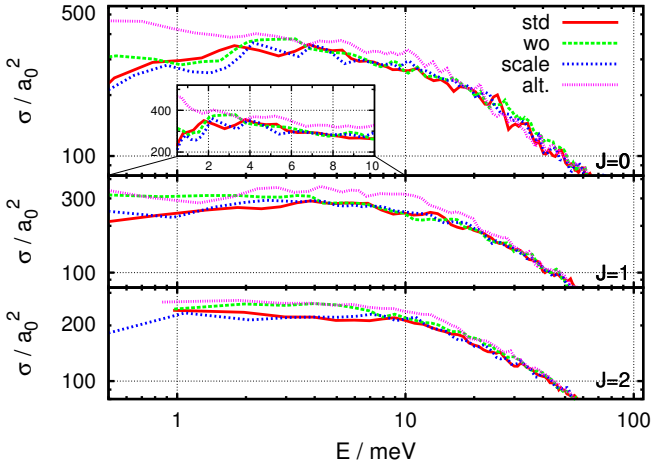

Fig. 12 Comparison of ABC quantum scattering abstraction cross sections for initial rotational quantum numbers 0 to 2. std = standard fit in this work, wo = standard fit without conical intersection terms, scale = standard potential scaled by 1.01 to fit D_es, alt. = alternative fit using different parameters (see text).

One major concern with *ab initio* based dynamics is the quality of the potential fit. Diagnostics of the fit can be done in several ways: e.g. visually, fit errors or comparison with experimental data. Another way is to perform exploratory studies on different fits. For this we performed ABC quantum scattering calculations for J=0 to 2 with collisional energies up to 100 meV. We used the fit used in this work (std), the same fit without the extra polynomials for the conical intersection (wo), the original fit scaled by 1.01 (scale) to fit experimental dissociation energies and an alternative fit (alt.). The alternative fit is 7th order two-body polynomial and 12th order three-body polynomial. The damping ranges λ were changed from $12\,a_0$ and $8\,a_0$ to $10\,a_0$ for both n-body terms. Figure 12 shows the respective cross sections. The scaled potential does

not show any significant change of the cross sections. While the dissociation energy D_e is an indicator for the overall quality of the *ab initio* data, this value is not important for the (low energy) dynamics. It seems, that a scaling of 1 % produces only minor changes in the gradients which govern the dynamics. This also suggests, that the usage of larger basis sets, like aug-cc-pVQZ, will not significantly improve the quality of the potential, assuming that no additional features are introduced. The comparison of our fit with the version which ignores the conical intersection shows increased cross sections for energies below 10 meV. While this can be seen easily for J=1 and 2, this effect is more hidden for J=0. In this figure it can be seen as a maximum around 3 meV. The influence of the conical intersection on the dynamics appears to be rather small, which corresponds to the small fraction of the configuration space of the incoming channel which is perturbed by the intersections and avoided crossings.

The largest change we find in the comparison with the alternative 12th order fit. Here the low energy cross sections are increased. Such deviations can be expected from the root mean square errors of the fits between 10 meV and 20 meV, while these errors do not state how strong the uncertainties of the cross sections are. The deviations are found to be about 10 %. Also the low energy limit is more horizontal. Extrapolated to the rate constants this would mean an uncertainty of approximately 10 % at the lower limit which decreases with temperature and should be negligible above 50 K.

References

1 E. Picazzio, A. De Almeida, S. M. Andrievskii, K. I. Churyumov and I. V. Luk'yanyk, Proceedings of Asteroids, 2002, pp. 713–716.

2 A. E. Douglas and G. Herzberg, *Astrophysical Journal*, 1941, **94**, 381.

3 T. Stoecklin and P. Halvick, *Phys Chem Chem Phys*, 2005, **7**, 2446–2452.

4 P. Halvick, T. Stoecklin, P. Larrgaray and L. Bonnet, *Phys. Chem. Chem. Phys.*, 2007, **9**, 582–590.

5 R. Plasil, T. Mehner, P. Dohnal, T. Kotrik, J. Glosik and D. Gerlich, submitted.

6 private communication with D. Gerlich.

7 D. Gerlich, G. Borodi, A. Luca, M. C. and M. A. Smith, *Zeitschrift für Physikalische Chemie*, 2011, **225**, 475–492.

8 H.-J. Werner and P. J. Knowles, *The Journal of Chemical Physics*, 1988, **89**, 5803–5814.

9 P. J. Knowles and H.-J. Werner, *Chemical Physics Letters*, 1988, **145**, 514 – 522.

10 P. J. Knowles and H.-J. Werner, *Theoretical Chemistry Accounts: Theory, Computation, and Modeling (Theoretica Chimica Acta)*, 1992, **84**, 95–103.

11 T. H. Dunning, *Journal of Chemical Physics*, 1989, **90**, 1007 – 1023.

12 R. A. Kendall, J. Thom H. Dunning and R. J. Harrison, *The Journal of Chemical Physics*, 1992, **96**, 6796–6806.

13 P. J. Knowles and H.-J. Werner, *Chemical Physics Letters*, 1985, **115**, 259 – 267.

14 H.-J. Werner and P. J. Knowles, *The Journal of Chemical Physics*, 1985, **82**, 5053–5063.

15 H.-J. Werner, P. J. Knowles, R. Lindh, F. R. Manby, M. Schütz, P. Celani, T. Korona, A. Mitrushenkov, G. Rauhut, T. B. Adler, R. D. Amos, A. Bernhardsson, A. Berning, D. L. Cooper, M. J. O. Deegan, A. J. Dobbyn, F. Eckert, E. Goll, C. Hampel, G. Hetzer, T. Hrenar, G. Knizia, C. Köppl, Y. Liu, A. W. Lloyd, R. A. Mata, A. J. May, S. J. McNicholas, W. Meyer, M. E. Mura, A. Nicklass, P. Palmieri, K. Pflüger, R. Pitzer, M. Reiher, U. Schumann, H. Stoll, A. J. Stone, R. Tarroni, T. Thorsteinsson, M. Wang and A. Wolf, *MOLPRO, version 2009.1, a package of ab initio programs*, 2009, see www.molpro.net.

16 X. Huang, B. J. Braams and J. M. Bowman, *Journal of Chemical Physics*, 2005, **122**, 1–12.

17 Z. Jin, B. J. Braams and J. M. Bowman, *Journal of Physical Chemistry A*, 2006, **110**, 1569 – 1574.

18 A. Sharma, J. Wu, B. Braams, S. Carter, R. Schneider, B. Shepler and J. Bowman, *Journal of Chemical Physics*, 2006, **125**, 224306.

19 Y. Wang, S. Carter, B. J. Braams and J. M. Bowman, *The Journal of Chemical Physics*, 2008, **128**, 071101.

20 Y. Wang, B. J. Braams, J. M. Bowman, S. Carter and D. P. Tew, *The Journal of Chemical Physics*, 2008, **128**, 224314.

21 J. N. Murrell, S. Carter, S. Farantos, P. Huxley and A. Varandas, *Molecular Potential Functions*, John Willey & Sons, 1985.

22 C. W. Gear, *Communications of the ACM*, 1966, **9**, 475–&.

23 L. Bonnet and J. C. Rayez, *Chemical Physics Letters*, 2004, **397**, 106–109.

24 L. Bonnet and J. C. Rayez, *Chemical Physics Letters*, 1997, **277**, 183–190.

25 L. Bonnet and C. Crespos, *Phys. Rev. A*, 2008, **78**, 062713.

26 L. Bonnet and C. Crespos, *Phys. Rev. A*, 2009, **80**, 059903.

27 R. A. Marcus, *The Journal of Chemical Physics*, 1971, **54**, 3965–3979.

28 W. H. Miller, *Adv. Chem. Phys.*, 1974, **25**, 69.

29 W. H. Miller, *The Journal of Physical Chemistry A*, 2001, **105**, 2942–2955.

30 D. Skouteris, J. F. Castillo and D. E. Manolopoulos, *Computer Physics Communications*, 2000, **133**, 128–135.

31 N. Sathyamurthy, *Chemical Reviews*, 1983, **83**, 601–618.

32 L. B. Harding, R. Guadagnini and G. C. Schatz, *The Journal of Physical Chemistry*, 1993, **97**, 5472–5481.

33 A. Luca, G. Borodi and D. Gerlich, Photonic, Electronic and Atomic Collisions, 2006, pp. 494–501.

34 W. Federer, H. Villinger, F. Howorka, W. Lindinger, P. Tosi, D. Bassi and E. Ferguson, *Phys. Rev. Lett.*, 1984, **52**, 2084–2086.

35 W. Federer, H. Villinger, P. Tosi, D. Bassi, E. Ferguson and W. Lindinger, in *Molecular Astrophysics*, ed. G.H.F. Diercksen *et al.*, D. Reidel Publishing Company, 1985, ch. Laboratory studies of ion reactions with atomic hydrogen, p. 649.

36 L. Bañares, F. J. Aoiz, P. Honvault and J. M. Launay, *Journal of Physical Chemistry A*, 2004, **108**, 1616–1628.